Self-organized multi-layered graphene-boron-doped diamond hybrid nanowalls for high-performance electron emission devices

Peer-reviewed author version

KAMATCHI JOTHIRAMALINGAM, Sankaran; Ficek, Mateusz; Kunuku, Srinivasu; Panda, Kalpataru; Yeh, Chien-Jui; Park, Jeong Young; Sawczak, Miroslaw; Michalowski, Pawel Piotr; Leou, Keh-Chyang; Bogdanowicz, Robert; Lin, I-Nan & HAENEN, Ken (2018) Self-organized multi-layered graphene-boron-doped diamond hybrid nanowalls for high-performance electron emission devices. In: NANOSCALE, 10(3), p. 1345-1355.

DOI: 10.1039/c7nr06774g
Handle: http://hdl.handle.net/1942/26543

Nanoscale

Accepted Manuscript

This article can be cited before page numbers have been issued, to do this please use: K. J. Sankaran, M. Ficek, S. Kunuku, P. Kalpataru, C. Yeh, J. Y. Park, M. Sawczak, P. P. Michaowski, K. Leou, R. Bogdanowicz, I. Lin and K. Haenen, *Nanoscale*, 2017, DOI: 10.1039/C7NR06774G.

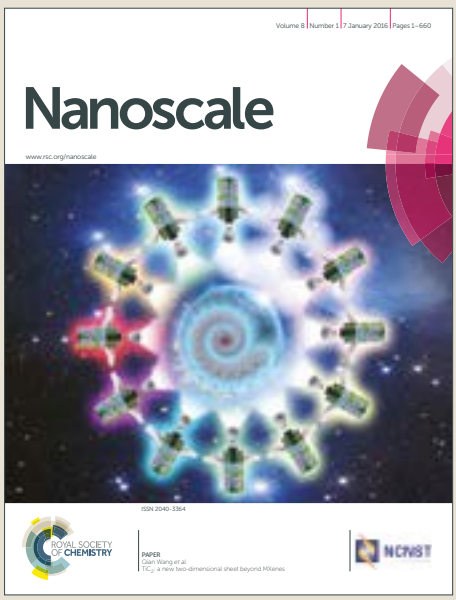

ROYAL SOCIETY OF CHEMISTRY

rsc.li/nanoscale

View Article Online
DOI: 10.1039/C7NR06774G

Self-organized multilayered graphene–boron doped diamond hybrid nanowalls for high performance electron emission devices

Kamatchi Jothiramalingam Sankaran,[*a,b] Mateusz Ficek,[c] Srinivasu Kunuku,[d] Kalpataru Panda,[e,f] Chien-Jui Yeh,[d] Jeong Young Park,[e,f] Miroslaw Sawczak,[g] Paweł Piotr Michałowski,[h] Keh-Chyang Leou,[d] Robert Bogdanowicz,[c] I-Nan Lin,[i] and Ken Haenen[*a,b]

[a]*Institute for Materials Research (IMO), Hasselt University, 3590 Diepenbeek, Belgium*

[b]*IMOMEC, IMEC vzw, 3590 Diepenbeek, Belgium.*

Email: sankaran.kamatchi@uhasselt.be, ken.haenen@uhasselt.be

[c]*Department of Metrology and Optoelectronics, Faculty of Electronics, Telecommunications and Informatics, Gdansk University of Technology, 11/12 G. Narutowicza St., 80-233 Gdansk, Poland*

[d]*Department of Engineering and System Science, National Tsing Hua University, Hsinchu, 30013 Taiwan, Republic of China.*

[e]*Center for Nanomaterials and Chemical Reactions, Institute for Basic Science (IBS), Daejeon, 34141 Korea.*

[f]*Graduate School of EEWS, Korea Advanced Institute of Science and Technology (KAIST), Daejeon, 34141 Korea.*

[g]*Center for Plasma and Laser Engineering, The Szewalski Institute of Fluid Flow Machinery, Polish Academy of Sciences, Fiszera 14, 80-231 Gdansk, Poland*

[h]*Institute of Electronic Materials Technology, Wólczyńska 133, 01-919 Warsaw, Poland.*

[i]*Department of Physics, Tamkang University, Tamsui, 251 Taiwan, Republic of China.*

Carbon nanomaterials like nanotubes, nanoflakes/nanowalls and graphene have been used as electron sources due to their superior field electron emission (FEE) characteristics. Nevertheless, these materials show poor stability and a short lifetime, preventing them from being used in practical device applications. The intention of this study was to find an innovative nanomaterial,

View Article Online
DOI: 10.1039/C7NR06774G

possessing both high robustness and reliable FEE behavior. A hybrid structure of self-organized multilayered graphene (MLG)–boron doped diamond (BDD) nanowall materials with superior FEE characteristics are successfully synthesized using a microwave plasma enhanced chemical vapor deposition process. Transmission electron microscopy reveals that the carbon clusters thus prepared are of uniform, dense and sharp nanowall morphology with sp^3 diamond cores encased by an sp^2 MLG shell. Detailed nanoscale investigations by peak force-controlled tunneling atomic force microscopy show that each of the core-shell structured carbon clusters field emits electrons equally well. The MLG-BDD nanowall materials show a low turn-on field of 2.4 V/μm, a high emission current density of 4.2 mA/cm^2 at an applied field of 4.0 V/μm, a large field enhancement factor of 4500 and prominently high lifetime stability (lasting for 700 min), enlightening their superiority on comparison with other hybrid nanostructured materials. The potential in practical device applications for these MLG–BDD hybrid nanowall materials is further illustrated by the plasma illumination behavior of a microplasma device, which used these materials as cathode, where low threshold voltage of 330 V (low threshold field of 330 V/mm) and long plasma stability of 358 min are demonstrated. The fabrication of these hybrid nanowalls is straight forward and thereby opens up a pathway for the advancement in next generation cathode materials for high brightness electron emission and microplasma-based display devices.

Keywords: multilayered graphene, boron doped diamond, hybrid nanowalls, self-organized, field electron emission, plasma illumination

1. Introduction

View Article Online
DOI: 10.1039/C7NR06774G

Electron emission sources are omnipresent in modern society and play a significant role in information displays. Carbon-based cold cathode materials like carbon nanotubes, carbon nanoflakes/nanowalls, graphene and diamond thin films, possess a low turn-on field and a high emission current density and are strongly anticipated for applications in field electron emission (FEE) based devices such as flat panel displays, electron microscope's gun, vacuum microelectronic devices and X-ray sources.[1–6] However, FEE is a complicated process and the FEE efficiency is decided by a combination of several factors, comprising conductivity of the emitter, resistance of the emitter/substrate interface, low work function of the emitting surface, sharpness of the emitting tip, stability at high emission current, and robustness of the emission materials surface.[7] Even though many field electron emitters emit electrons proficiently, they struggle with temporal stability of the current at high electric fields corresponding to operative conditions. Therefore, the fabrication of a high performance cold cathode emitter with extended lifetime is the foremost challenge for practical device applications.

Nano-carbon hybrid structures that integrate two carbon allotropes with each of them possessing unique and outstanding properties, generate much attention because of their synergistic electronic behavior. Predominantly when combining sp^2 and sp^3 bonds, like "graphene–diamond hybrids" and "CNTs–diamond hybrids".[8–10] Graphene, monolayered sp^2-bonded carbon atoms in a honeycomb crystal lattice and high chemical stability, possess highly desirable properties, such as high mobility of charge carriers, outstanding electrical and thermal conductivity, high aspect ratio and sharp edges, creating it a suitable material for FEE applications.[11,12] However, the FEE efficiency from graphene nanosheets is unsatisfactory due to poor stability and short lifetime of the graphene emitters,[13,14] preventing them from being utilized in practical applications.

View Article Online
DOI: 10.1039/C7NR06774G

Conversely, diamond with strong covalently sp^3-bonded crystal structure, possessing high hardness, high chemical inertness, and negative electron affinity (NEA)[15] can be a good candidate for high reliability solid-state electronic emitters, especially when H-terminated. Moreover, the intrinsic insulating nature of diamond, which limits the FEE efficiency, can be improved effectively by *p*-type (e.g. boron)[16,17] or *n*-type (e.g. nitrogen, phosphorus)[18,19] doping. In particular, boron doped diamond possesses excellent electrical conductivity and robustness concede some outstanding performances.[20] As a result, it is recommended to integrate graphene and boron doped diamond to form hybrid nanostructures with enhanced FEE characteristics, as such hybrids are known to have the advantages of both high stability of diamond and high field emission characteristics of graphene materials.

To this end, the current work focused on the synthesis of self-organized multilayered graphene (MLG)–boron doped diamond (BDD) hybrid nanowall materials using a microwave plasma enhanced chemical vapor deposition (MWPECVD) process. Practically, these *in-situ* grown hybrid nanowalls can be used as cathodes for FEE and microplasma cathode devices. A noticeable improvement in the FEE and plasma illumination (PI) characteristics as well as good lifetime stability of the related devices was achieved. Such hybrid nanowall material, which possesses simultaneously superior FEE/PI characteristics and good robustness possess immense potential for practical device applications.

2. Results

Material's characteristics: The scanning electron microscopy (SEM) image shown in Figure 1a clearly reveals the nanowall-like structures for the MLG-BDD materials. They contain carbon clusters with compact and curled morphology of nanowalls with lengths around 1–3 μm. The inset "I" in this figure indicates that the nanowalls are about 3.0 μm in height for the growth time

View Article Online
DOI: 10.1039/C7NR06774G

of 6 h, whereas the inset "II" in this figure shows the three-dimensional (3D) reconstruction SEM image, revealing that the thickness of nanowalls is around 80–100 nm. At the top of the nanowalls sharp edges are present. Furthermore, Figure 1b presents secondary ion mass spectrometry (SIMS) mapping of the top (Figure $1b_1$) and bottom (Figure $1b_2$) parts of the sample. The boron concentration is about two times higher for the top part of the nanowalls than for the solid carbon layer close to the Si substrate, confirming the successful incorporation of boron in the nanowalls.[21]

Raman spectrum (λ = 514 nm) of MLG-BDD nanowall materials shown in Figure 1c illustrates that the carbon clusters contain a prominent peak of the D band at around 1350 cm^{-1}, which is associated with disordered sp^3-hybridized carbon featured as defects or impurities in carbon materials, the G band around 1584 cm^{-1}, which is associated with E_{2g} phonon modes of the sp^2-bonded carbon and a broad 2D peak around 2700 cm^{-1} originated from a second-order process. The I_{2D}/I_G ratio is about 0.23, indicating that the carbon clusters are ultra-thin multilayered graphene.[22] An inconspicuous band (D+G) at 2938 cm^{-1} is owing to the defects in sp^2 sites and graphene domain edge in the MLG.[23] The presence of a broad peak at around 480 cm^{-1} is related to boron modified carbon nanosheets.[24]

X-ray photoelectron spectroscopy (XPS) measurements were carried out to reveal more clearly the surface chemical bonding characteristics of MLG-BDD hybrid nanowall materials. Figure 1d describes the typical C1s core level spectral line for these materials, after the background was subtracted using Shirley's method.[25] The curves were fitted by the Lorentzian peaks at their corresponding binding energies of sp^2 C=C (~283.8 eV), sp^3 C−C (~285.0 eV), C=N (~286.0 eV) and C−O (~287.3 eV).[26] The spectrum reveals that the carbon clusters are

View Article Online
DOI: 10.1039/C7NR06774G

predominated with sp^2 C=C bonding (peak intensity of 63.6%) and sp^3 C−C (peak intensity of 32.5%). The presence of C=N (2.3%) signifies the existence of nitrogen in the sample. A little amount of C-O peaks (1.6%) is seen in binding energy of 286.1 eV. The B1s spectrum (inset "I" of Figure 1d) shows only one component at 187.2 eV,[27] which confirms the presence of boron in the nanowalls. This observation is in agreement with the SIMS results (cf. Figure 1b). Moreover, the N1s spectrum (at ~ 402 eV) in the inset "II" of Figure 1d indicates that incorporation of N_2 into the structure of nanowalls is very weak. Notably, these carbon clusters contain higher proportion of sp^3-bonded carbon (32.5%) than the conventional carbon nanowalls (18.5%).[28]

FEE behavior: FEE measurements were carried out on the MLG-BDD nanowall materials using a set-up illustrated schematically as the inset of Figure 2a. The FEE results are displayed in Figure 2a, whereas the turn-on field (E_0) is defined as the electric field necessitated for generating a FEE current density (J_{FEE}) of 10 μA/cm^2. MLG-BDD nanowall materials possess superior FEE properties demonstrating a low E_0 value of 2.4 V μm^{-1} and high J_{FEE} of 4.2 mA cm^{-2} at an applied field of 4.0 V μm^{-1}. These measurements were reproducible at different locations on the same sample, indicating that the FEE behavior is rather uniform over the MLG-BDD hybrid nanowall materials.

The FEE process from a material was generally modeled by Fowler-Nordheim (F-N) theory,[29] viz. the electrons were tunneling through a potential barrier (work function, φ) and the emission current density (J_{FEE}) can be expressed as follows:

$$J_{FEE} = (A\beta^2E^2/\varphi) \exp(-B\varphi^{3/2}/\beta E)$$

where A and B are constants with the values of 1.54×10^{-6} A eV V^{-2} and 6.83×10^9 eV$^{-3/2}$ V m^{-1}, respectively. β is the field-enhancement factor, E is the applied field and φ is the work function of the emitters. The inset of Figure 2b shows a linear relationship in F-N plot, i.e., ln (J_{FEE}/E^2)

View Article Online
DOI: 10.1039/C7NR06774G

versus ($1/E$) curves, corresponding to J_{FEE}-E curve in Figure 2a, indicating that the FEE process of MLG-BDD nanowall materials followed the F-N model agreeably.[7, 30–34] Generally, electrons were transported along the nanowalls toward the tip surface and emit from these protrusive regions, as they have smaller curvature radius (cf. insert "II" of Figure 1a) and of higher β factor. Normally, the β-value is dependent on the tip geometry and the aspect ratio of the nanostructures and can be estimated from the slope of F-N plots as follows: $\beta = -[B\,\varphi^{3/2}]/m$, where, m is the slope of F-N plots. Hence β for MLG-BDD nanowall materials is estimated to be ~4500 (or 6230) by taking the φ values of 5.0 eV (i.e., assuming the top-edge material is diamond)[35] or 4.62 eV (i.e., assuming the top-edge material is graphene).[36] Restated, the MLG-BDD hybrid nanowall materials exhibit far more efficient FEE properties, i.e., lower E_0, higher J_{FEE} and larger β values, than those of other diamond-based hybrid nanostructures (Table Ia)[37–43] and comparable FEE properties with the carbon nanoflakes/nanowalls (Table Ib).[44–54]

The long-term emission behavior, the lifetime stability, of a FEE device is an important parameter related to practical applications. Stability of the field emission current from MLG-BDD nanowall materials was evaluated at a J_{FEE} value of 2.0 mA cm^{-2}, which corresponds to a working field of 3.7 V μm^{-1}. The result is presented in Figure 2b. The difference between the initial (~2.004 mA cm^{-2}) and final (~1.999 mA cm^{-2}) emission current was observed to be negligible for a period of 700 min, implying that the lifetime stability of these carbon clusters could be better than this value. The robustness of MLG-BDD nanowall materials is comparable with that of the diamond-based nanostructures but MLG-BDD nanowall materials possess superior FEE behavior (cf. Table Ia)). The FEE stability of MLG-BDD nanowall materials is much better than those of carbon nanoflakes/nanowalls (cf. Table Ib), revealing the superiority of

View Article Online
DOI: 10.1039/C7NR06774G

these materials for practical device applications, even though the FEE properties of MLG-BDD hybrid nanowall materials are not as good as carbon nanoflakes/nanowalls.

Moreover, atomic force microscopy (AFM)-based peak force-controlled tunneling atomic force microscopy (PF-TUNA) measurements were performed on MLG-BDD hybrid nanowall materials to inspect the main conducting paths for electrons from the microscopic point of view. Basically, the PF-TUNA technique with the additional advantage of performing the experiment at a local scale on the sample surface is found to be a more representative picture of the electron emission scenario that reveal the exact electron emission sites and helps to understand better the interpretation of the field emission data for diamond and related materials.[55] In PF-TUNA measurements, the electrons is tunneling directly, from the surface through a 1 nm air gap into the tip, and the magnitude of tunneling current depend upon tip to sample separation. Figure 3a shows a typical AFM image of the MLG-BDD hybrid nanowall materials, revealing again the nanowall geometry of the carbon clusters. Figure 3b indicates the PF-TUNA current mapping corresponding to the AFM image in Figure 3a, which was taken at a sample bias of -1 V. The brighter contrast in the PF-TUNA image represents a high electron emission current. The shapes of the bright and dark regions in the PF-TUNA mapping in Figure 3b are similar to those in Figure 3a. The emission sites with markedly larger emission current are preferentially seen along the top surface of carbon clusters. To reveal the exact distribution of the electron emission sites in a local scale, the high-resolution AFM surface morphology is recorded (Figure 3c) with the corresponding PF-TUNA current mapping shown in Figure 3d, which was measured at a sample bias of -2 V. The PF-TUNA micrograph in Figure 3d shows that every nanowall carbon clusters emits electrons equally well. There appears to be a finer structure in the PF-TUNA image (Figure 3d) than the AFM topographic micrograph in Figure 3c. These results

View Article Online
DOI: 10.1039/C7NR06774G

imply that the top-edges of MLG-BDD nanowall materials (designated as "t_1", "t_2" and "t_3") emit more electrons than the side-walls (designated as "w_1", "w_2" and "w_3"). A recent investigation of electron emission sites from BDD films using PF-TUNA technique by Harniman *et al.* supports our findings that doping with boron increases the grain conductivity and broadens the emitting grain-boundary sites so as the emission starts from the side-walls of the grains.[56]

Furthermore, local current-voltage (*I-V*) characteristics in the AFM-based PF-TUNA for the MLG-BDD nanowall materials were acquired to cross-check the local electron emission mappings behavior. The local *I-V* curves recorded during PF-TUNA scanning at the top edges and at side walls of MLG-BDD nanowall materials are shown, respectively, in Figure 3e. Fascinatingly, the tunneling current at the top edges (curve I) is much larger than that at the side walls (curve II) of MLG-BDD nanowall materials. Such a phenomenon can be ascribed to the higher field concentration factor of the emission sites located at the top edges of carbon clusters. It should be mentioned that, in Figure 3e, eight reproducible *I-V* curves were recorded corresponding to each emission sites, indicating that electron emission behavior of each sites is reproducible.

Microstructure: The FEE properties of MLG-BDD nanowall materials are much better than those of diamond nanostructured based FEE emitters. These FEE characteristics are comparable with the nanoflakes/nanowalls but the MLG-BDD nanowall materials but exhibit superior robustness than the conventional nanoflakes/nanowalls. To understand the genuine factor ensuing in such superior FEE behavior, the microstructure of MLG-BDD nanowall materials was investigated using transmission electron microscopy (TEM). The inset "I" in Figure 4a shows the bright field TEM micrograph (BF-TEM) of the MLG-BDD nanowall materials, indicating that

View Article Online
DOI: 10.1039/C7NR06774G

the carbon clusters of nanowall geometry are uniform and densely distributed in the samples. Figure 4a shows the enlarged BF-TEM micrograph of the regions, which correspond to dotted squares "A" in inset "I" of Figure 4a, that illustrates more clearly the microstructure of these carbon clusters. High contrast of these carbon clusters show that they are well crystallized and diffract electrons strongly. A selective area electron diffraction (SAED) pattern shown in the inset "II" of Figure 4a reveals the presence of strong diffraction ring (designated as "G" and indicated by the arrow), which corresponds to the graphene (G) phase, revealing that these materials are predominately the graphene phase. There also exists a strong diffuse ring in the center of SAED, which corresponds to amorphous carbon. Additionally, faint ring patterns appear corresponding to the (111), (220), and (311) lattice planes of diamond, which clearly illustrates the presence of diamond in these carbon clusters of nanowall materials. Notably, only when the crystalline carbon clusters are properly oriented (i.e., near a zone-axis), they can diffract electrons strongly, showing dark contrast. When they are oriented away from the zone-axis, they diffract electrons weakly, showing light (or grey) contrast.

The granular structure of these nanowall materials is more clearly revealed by the high resolution TEM micrograph. The TEM structure image shown in Figure 4b, which corresponds to the region designated by dotted square "B" in Figure 4a, reveals the presence of core-shell granular structure, i.e., with diamond core encased in MLG shell for each carbon clusters in nanowall materials, viz. each of the core-shell structured carbon clusters is a hybrid nanomaterials. The diamond core embedded in MLG shell microstructure is confirmed by the Fourier transformed (FT) diffractogram i corresponding to the entire structure image shown as an inset in Figure 4b. This FT image consists of a strong central diffuse ring with a donut appearance (designated as "G"), which is an indicative of the presence of graphene phase in

View Article Online
DOI: 10.1039/C7NR06774G

these materials. Moreover, faint diffraction spots are presented (designated as "D"), which correspond to the diamond core in these clusters. This micrograph implies that, for MLG-BDD hybrid nanowall materials, the diamond cores are very thin (~5 nm) and the MLG phases encasing the diamond cores are approximately tens of layers in thickness and highly crystallized. The encasing MLG phases have parallel fringes with an interlayer spacing of 0.34 nm, confirming the well crystalized graphite nature of the MLG phases.[23] The distribution of phase constituents in the MLG-BDD hybrid nanowall materials is better illustrated by the composed dark field (c-DF) image in Figure 4c, which is the superposition of several dark field images acquired using different diffraction spots (yellow and green circles, the inset "II" of Figure 4a). The yellow colored ring and the corresponding phase represent the diamond, whereas the green colored ring and the corresponding phase are the graphene phase. Fascinatingly, the c-DF image reveals that each of the carbon clusters contains diamond cores, viz. the MLG-BDD is actually a hybrid nanowall material.

The local bonding characteristics of these carbon clusters are analyzed using electron energy loss spectroscopy (EELS) in TEM. The core-loss EELS spectrum in the carbon K-edge region for MLG-BDD hybrid nanowall materials, which corresponds to BF-TEM micrograph in Figure 4a, was recorded. Figure 4d signifies that besides a sharp peak at 289.5 eV (σ* band) and a dip valley in the vicinity of 302.0 eV,[57] there occurs a large bump at 285.0 eV (π* band). The σ* band and the dip valley signify the sp^3-bonded carbon (the diamond), whereas the π* band characterizes the sp^2-bonded carbon.[57–59] The nature of the sp^2-bonded carbon materials comprised in the carbon clusters was further examined using plasmon-loss EELS, which is shown as an inset in Figure 4d. This spectrum discloses that the sp^2-bonded carbon present in these carbon clusters is graphitic in nature, since it contains a large diffuse peak at 27.0 eV.[60,61]

View Article Online
DOI: 10.1039/C7NR06774G

These micrographs again imply that each carbon clusters in MLG-BDD nanowall materials is actually a nanocarbon hybrid material, consisting of diamond as core and MLG as shell. The TEM and EELS observations are in concurrence with the Raman and XPS investigations.

High quality field emitters have recently enlarged significance because of their prospective for consistent integration into optoelectronic devices. Predominantly, microplasma based devices signify a photonics technology at the connection of plasma science, optoelectronics, and materials science and display a promising future applied to a broad spectrum of applications such as microdisplay panels, ozone production, detectors of environmentally hazardous gases or vapors, and numerous bioelectronics and biomedical applications.[62–64] Several cold cathode materials, e.g. Mo, CNTs, ZnO and Si achieve splendidly in emission of electrons which were established for these microplasma device applications.[65–68] Nevertheless, these materials and the related microplasma device suffer from stability issues,[69–71] as the cathode materials in these devices are subjected to continuous plasma ion bombardment during the operation of the devices that is considered to be the harshest environment in device applications. Therefore, materials possessing good robustness (long lifetime and reliability), yet possess large secondary electron emission efficiency (γ-coefficient) are required for serving as cathode for these devices. Furthermore, reported simulation works[72,73] anticipated that high FEE cathode materials can noticeably increase the performance of microplasma device characteristics. MLG-BDD hybrid nanowall materials possess superior FEE properties as well as robustness are the most favorable cathode materials as the diamond core also own high γ-coefficient. To shed light on the potential of these materials in device application, the PI properties of a microplasma device, which used these materials as a cathode were investigated. A schematic diagram of the microplasma measurement set-up is shown in the inset of Figure 2c. Inset “I” in Figure 2d shows

View Article Online
DOI: 10.1039/C7NR06774G

the PI images of the microplasma devices, indicating that the microplasma devices can be ignited at a low voltage of 330 V, which corresponds to a threshold field (E_{PI}) of 0.33 V μm^{-1} and the brightness of the PI images increases monotonically with the applied voltage. The performance of the microplasma devices is better demonstrated from plasma current density–applied field (J_{PI}–E) curve in Figure 2c. This curve indicates that the J_{PI} increases from 1.6 mA cm^{-2} at an applied field of 0.33 V μm^{-1} (330 V applied voltage) to around 6.0 mA cm^{-2} at 0.51 V μm^{-1} (510 V applied voltage). Furthermore, the microplasma devices employing these cathode materials were examined over an extensive period with a constant applied field of 0.37 V μm^{-1} (370 V applied voltage) to evaluate their lifetime stability. Figure 2d establishes that the microplasma devices using MLG-BDNWs hybrid nanowalls as cathode can last more than 21500 s (358 min) under a tested current density of J_{PI}=2.40 mA cm^{-2} (at E=0.37 V μm^{-1}). The inset "II" of Figure 2d shows that the intensity of the PI of these hybrid nanowalls at 0.37 V μm^{-1} remains stable after this test period (i.e., 358 min) that illustrates the high stability of these hybrid nanowalls. This performance is better than the microplasma devices which used other kind of diamond emitters as cathode.[37–43] Notably, the carbon nanoflakes/nanowalls is extremely susceptible to the plasma ion bombardment damage and is totally not applicable for the microplasma device applications.

3. Discussion

To understand the growth mechanism of the core-shell structured carbon clusters, optical emission spectroscopy (OES) spectrum analysis was carried out for the $H_2/CH_4/B_2H_6/N_2$ based growth plasma.[74] The OES spectrum shown in Figure 5 reveals the presence of H, CN, H_yCNH_x, BH_x and C_2 species in the plasma, which could be responsible for the formation of MLG-BDD

View Article Online
DOI: 10.1039/C7NR06774G

nanowalls growth. The growth mechanism and specific core-shell structure depend on the pre-growth seeding procedure and surface chemistry during MPECVD process. Our recent observations revealed that diamond core of MLG-BDDs originated from overgrown nanodiamond grains used for seeding procedure and by C_2 species. The C_2 species renucleate new diamond clusters, resulting in ultra-small grains granular structure.[75] The graphene shells are attributed to the degenerated growth of diamond phase caused mainly by BH and HCN species.[76] The joint studies utilizing optical emission of plasma along with Raman spectroscopy and XPS proved that molecular geometry and higher electron−ion recombination rates of H_yCNH_x species could be responsible for the described edge growth of multilayer graphene nanowalls.[61] Moreover, the relatively high contribution of dense diamond core could be also the results of bombardment of surface by highly energetic ions modifying local density by sub-plantation of particles (direct or knock-on).[77] Last but not least, HNC-C bonding possesses here the lowest bond energy of 389.0 eV. Furthermore, the BH_x radicals are probably responsible for developed morphology of wall-like shape or length.[78,79] However, the formation process for such a core-shell structured carbon clusters is rather complicated. The understanding on genuine mechanism requires more systematic investigation.

Concerning the superior FEE properties of MLG-BDD hybrid nanowall materials, H. D. Li[80] *et al.* recently investigated the electronic properties of thin diamond slab using first-principles calculations and revealed that these thin slabs possess electronic characteristics of diamond, i.e., wide bandgap (E_g=5.3 eV) and insulating properties when the number of (111) diamond layers in the thin slab is larger than 12. However, when the number of (111) layers is smaller than 11, the bonding of most surface layer become unstable and this layer was transformed from sp^3 to sp^2. This layer has slightly larger spacing with the adjacent (111)

View Article Online
DOI: 10.1039/C7NR06774G

diamond lattice plane than the normal (111) lattice spacing. Moreover, such kind of "extremely thin diamond slab" shows a gapless electronic structure (E_g~0 eV) and a semimetal properties like a single layer graphene material. Stacking of more graphene-like layer on top of it does not modify such a characteristic. That is the diamond slab was transformed from wide band gap insulating materials into gapless semimetal ones (it can be *p*-type or *n*-type conducting depends on the position of the Fermi level with respect to the Dirac point). Such a behavior could be more important factor, rendering the MLG-BDD hybrid materials superior FEE behavior. The high conductivity of MLG-BDD hybrid materials is not just coming from the presence of highly conducting graphene-like shell, encasing the insulating diamond core. It is the quantum interaction of the electronic orbits between these two materials that convert the materials into very conducting nano-hybrids. Although the phenomenon that "ultra-thin diamond slab" possess a gapless electronic structure and thus exhibit markedly better conductivity than the conventional diamond films has not been directly confirmed by experiments, such a model can explain the high robustness of the core-shell structured carbon nano-clusters. The arguments are described as follows:

Comparison of Tables Ia and Ib infers that the carbon nanoflakes/nanowalls based emitters show better FEE properties but with inferior lifetime stability, compared with the diamond nanostructure based emitters. This implies that, in general, the material's robustness can be improved only at the expense of sacrificing the FEE behavior. It is intriguing to observe that, for MLG-BDD hybrid nanowall materials, the unique granular structure improved significantly the FEE lifetime stability but without markedly degrading the FEE properties of the materials (table Ic). The question to be answered is how does the unique microstructure of carbon clusters, MLG-BDD hybrid nanowall materials, support these intriguing properties of low turn-field and high

View Article Online
DOI: 10.1039/C7NR06774G

FEE current density behavior yet maintaining high robustness. While the high electron conductivity of the carbon clusters is understandable as they are the inherited nature of the well crystallized graphene-like materials, it cannot be explained in a straight forward way about how do these sp^2-bonded carbon clusters resist the degrading process during the field emission and microplasma operations. Apparently, it is closely related to the unique core-shell granular structure of the carbon clusters, viz. the MLG-BDD hybrid nanowall materials contain a diamond core embedded in an MLG shell. The sp^3-bond nature of diamond core is known to be extremely strong and can survive all kinds of degradation process such as bombardment damage of ionized gas molecular species originally adhered on the FEE emitters that were desorbed, ionized and accelerated toward emitting surface during FEE process. Although the MLG shell encasing the diamond core is expected to be susceptible to the erosion, the "ultra-thin diamond slab" will automatically convert the outmost (111) diamond lattice plan into sp^2-bonded carbon. The diamond grains remain highly conducting, showing no degradation of the FEE behavior of the MLG-BDD materials. Therefore, these materials show high lifetime stability along with superior FEE properties.

As to the role of boron on enhancing the field emission properties of boron doped diamond cores, several controversial models have been proposed for the electron emission mechanism from these films. Wisitsoraat *et al.*[81] had proposed that boron dopants increase the field enhancement due to the formation of hole accumulation via the formation of cascaded sp^2-diamond-sp^2 embedded microstructures. Other researchers proposed a FEE model from the sub-band.[82] Lee *et al*. reported that boron doping into the nanocrystalline diamond films does not result in consistent boron-content dependence of the FEE properties for the films as those in conventional micron-sized diamond films.[83] It is evident that the mechanisms derived to explain

View Article Online
DOI: 10.1039/C7NR06774G

the FEE enhancement due to boron doping are not totally clear. The other possible explanation on the enhancement of FEE behavior of the MLG-BDD hybrid nanowalls is the nanoscale dielectric inhomogeneity proposed by Carey's and Ilie's groups.[84–86] They demonstrated that sp^2 clusters embedded in the sp^3 matrix (or vice versa) induced by localized defects oriented in the field direction can provide a local field enhancement to facilitate the emission. As a consequence, in the present hybrid nanowalls, conductive spatially localized sp^2-MLG phase surrounding the nanowall-like sp^3-diamond cores, giving rise to dielectric inhomogeneity that lead to an enhanced local field at the vertically aligned sharp tips those facing the anode as is indicated by the high β-value. Additionally, the diamond cores protect the emitter from ion bombardment during operation, thus a high field emission current stability, i.e., high robustness is sustained.

4. Conclusions

In conclusion, we demonstrated a scalable and reproducible process for synthesizing MLG-BDD hybrid nanowalls on Si substrates with long lifetime stability of FEE and PI performances. The SEM and TEM analyses depict the nanowall morphology feature with a length of few hundred nanometers. The SAED pattern and Raman spectrum specify the co-occurrence of diamond and MLG phases. The XPS spectrum endorsed the introduction of boron and nitrogen into the nanowalls. Furthermore, the HRTEM image disclosures that the nano-sized carbon clusters in nanowalls contain randomly oriented diamond as cores and MLG layers as shell, encasing the diamond cores. The PF-TUNA measurements show more emission sites from each of the top surface of MLG-BDD carbon clusters. Moreover, this material exhibits a low E_0 of 2.4 V μm^{-1} with high J_{FEE} of 4.2 mA cm^{-2} (at an applied field of 4.0 V μm^{-1}) and a large β of 4500. The

View Article Online
DOI: 10.1039/C7NR06774G

hybrid film exhibits good FEE current stability of 700 min and is better than that of the carbon-based based hybrid FEE materials and have greater potential for device applications. The potential for practical device applications of these high performance FEE materials is demonstrated by the PI measurements for a microplasma device using these materials as cathode. The microplasma device developed from these hybrid nanowall materials as cathodes are able to generate plasma at a low threshold voltage of 330 V and high plasma stability of 358 min. Overall, this novel hybrid nanostructure with highly enhanced FEE and PI properties has the potential to combine the major advantages of its individual components to produce significant improvement in the fabrication of high brightness FEE display and microplasma-based devices with long lifetimes.

5. Experimental section

A MWPECVD system (2.45 GHz, SEKI Technotron AX5400S, Japan) was used for the synthesis of MLG-BDD hybrid nanowall materials using $H_2/CH_4/B_2H_6/N_2$ gas mixtures. A more detailed deposition procedure has been published elsewhere.[74] Briefly, prior to the nanowall growth, polished Si <100> substrates were seeded with slurry of DMSO-based nanodiamond particles of size ~5 nm, yielding a high seeding density of 10^{10} cm^{-2}. The gas flow rate, gas pressure, microwave power and growth time were 328 sccm, 50 Torr, 1.3 kW and 6 h, respectively. The substrate holder was heated by an induction heater to around 700°C, which was controlled by a thermocouple.

The morphology of the MLG-BDD hybrid nanowall materials was examined using SEM (EVO-40, Zeiss, Germany) with 10 kV beam accelerating voltage. 3D reconstruction of SEM image was performed in http://gwyddion.net/ where the scale of grey color was calibrated as

View Article Online
DOI: 10.1039/C7NR06774G

depth. A CAMECA SC Ultra instrument was used for SIMS imagining. An O^{2+} primary beam was rastered over 50 × 50 μm, whereas the positive ion detection was used for SIMS measurements. The beam intensity was set to 30 pA for imaging and 110 nA for sputtering. The analysis area was limited to 20 × 20 μm. To obtain sufficient lateral resolution, amorphous carbon was coated on the sample prior to the SIMS analysis. The crystalline quality of the MLG-BDD nanowall materials was characterized by using a micro-Raman system (InVia, Renishaw, UK; λ = 514 nm argon ion laser excitation). The chemical bonding of the surface of the MLG-BDD nanowall materials was examined using XPS (Sigma probe-Thermo VG Scientific) equipped with a hemispherical analyzer and microfocused monochromator X-ray source, Al Kα radiation (E = 1486.6 eV) with an energy resolution of 0.47 eV, in ultra-high vacuum at 10^{-10} Torr. The detailed microstructure and local bonding structure of the MLG-BDD nanowall materials were examined by TEM (Jeol 2100F) and EELS (Gatan Enfina) in TEM, respectively. To analyze the constituents in the plasma, the OES spectrum was recorded with a 0.3 m monochromator (SR303i, Andor) equipped with a 1200 groves/mm grating and ICCD detector (DH740, Andor).

FEE measurements were carried out using a homemade tunable parallel-plate capacitor set-up using Mo rod of 2 mm in diameter as an anode. The cathode-to-anode distance was controlled by a micrometer and an optical microscope. The *I-V* characteristics were measured at a pressure below 10^{-6} Torr with Keithley 2410 source meter. The PF-TUNA measurements were performed at ambient conditions using a multi-mode VIII AFM with a Nanoscope V controller and PF-TUNA module [Bruker, CA, USA]. The measurement details have been explained elsewhere.[87] Briefly, the base of the Si substrate was attached to a metallic disc using conductive silver paint (G3790 Agar Scientific) to make the electrical contact between the

View Article Online
DOI: 10.1039/C7NR06774G

MLG-BDD hybrid nanowall materials and the AFM tip. Topographic and tunneling current information were collected under PeakForce feedback. A Pt–Ir coating on the tip of the cantilever, with spring constant of 9.8 N/m, allowed the measurement of current when a bias was applied between the tip and sample. Images were recorded at a resolution of 512 × 512 pixels with a tip bias of a few volts at a lower scan rate (usually 0.1 or 0.2 Hz) to allow the maximum time for the TUNA current measurement in a particular position. A variety of tests were performed in this scenario to confirm that the measured TUNA current was a true reflection of the emission properties of the surface and not from any artifacts present on the surface. The recorded emission currents, with tip–sample biases varying from the mV to V range, were in the range of few pA to a few nA per emission site.

The PI characteristics of a microplasma device, using MLG-BDD hybrid nanowall materials as cathode, were also investigated. A cylindrical type microplasma device was made by using indium tin oxide (ITO) coated glass as anode and a Teflon spacer (1.0 mm in thickness) to fix the cathode-to-anode separation. A circular hole (diameter~ 3.0 mm) was cut out from the Teflon spacer to form a cylindrical microcavity. The device was kept in a vacuum chamber with a base pressure of 0.01 mTorr and the microplasma was ignited by using a DC pulsed voltage under 2 Torr of Ar (10 sccm). In order to improve the reliability of the measurements, the samples were heated at 200°C for 1 h before the measurements to remove moisture on the surface of the samples. The J_{PI}–E characteristics were acquired using a Keithley 2410 electrometer. The plasma was observed through the transparent anode by a USB microscope and snapshots were taken for different voltages to characterize the PI behavior of the microplasma device.

Conflicts of interest

View Article Online
DOI: 10.1039/C7NR06774G

There are no conflicts to declare.

Acknowledgements

The authors like to thank the financial support of the Research Foundation Flanders (FWO) via Research Grants 12I8416N and 1519817N, and the Methusalem "NANO" network. K. J. Sankaran is a Postdoctoral Fellow of the Research Foundation-Flanders (FWO). This work is also supported by the Polish National Science Centre (NCN) under Grant Nos. 2014/14/M/ST5/00715 and 2016/21/B/ST7/01430. The DS funds of Faculty of Electronics, Telecommunications and Informatics of the Gdansk University of Technology are also acknowledged. K. P. and J. Y. P. were supported by the Institute for Basic Science [IBS-R004-A2-2017-a00]. The manuscript was written through contributions of all authors. All authors gave approval to the final version of the manuscript.

References

1 E. Minoux, O. Groening, K. B. K. Teo, S. H. Dalal, L. Gangloff, J. P. Schnell, L. Hudanski, I. Y. Y. Bu, P. Vincent, P. Legagneux, G. A. J. Amaratunga and W. I. Milne, *Nano Lett.*, 2005, **5**, 2135.

2 C. H. Garcia, M. L. Stutzman and P. G. Oshea, *Phys. Today*, 2008, **61**, 44.

3 X. Yang, Z. Li, F. He, M. Liu, B. Bai, W. Liu, X. Qiu, H. Zhou, C. Li and Q. Dai, *Small*, 2015, **11**, 3710.

4 X. Zhang, L. Gong, K. Liu, Y. Cao, X. Xiao, W. Sun, X. Hu, Y. Gao, J. Chen, J. Zhou and Z. L. Wang, *Adv. Mater.*, 2010, **22**, 5292.

5 N. Shang, P. Papakonstantinou, P. Wang, A. Zakharov, U. Palnitkar, I. N. Lin, M. Chu, and A. Stamboulis, *ACS Nano*, 2009, **3**, 1032.

View Article Online
DOI: 10.1039/C7NR06774G

6 S. S. Fan, M. G. Chapline, N. R. Franklin, T. W. Tombler, A. M. Cassell and H. J. Dai, *Science,* 1999, **283**, 512.

7 O. Gröning, O. M. Küttel, C. Emmenegger, P. Gröning and L. J. Schlapbach, *J. Vac. Sci. Technol. B*, 2000, **18**, 665.

8 Y. Wang, M. Jaiswal, M. Lin, S. Saha, B. Ozylimaz and K. P. Loh, *ACS Nano*, 2012, **6**, 1018.

9 F. Zhao, A. Vrajitoarea, Q. Liang, X. Han, A. Chaudhary, J. O. Welch and R. B. Jackman, *Sci. Rep.*, 2015, **5**, 13771.

10 T. H. Chang, P. Y. Hsieh, S. Kunuku, S. C. Lou, D. Manoharan, K. C. Leou, I. N. Lin and N. H. Tai, *ACS Appl. Mater. Interfaces*, 2015, **7**, 27526.

11 I. Lahiri, V. P. Verma and W. Choi, *Carbon*, 2011, **49**, 1614.

12 D. M. Trucchi and N. A. Melosh, *MRS Bulletin*, 2017, **42**, 488.

13 W. T. Zheng, Y. M. Ho, H. W. Tian, M. Wen, J. L. Qi and Y. A. Li, *J. Phys. Chem. C*, 2009, **113**, 9164.

14 J. H. Deng, L. Cheng, F. J. Wang, D. J. Li and G. A. Cheng, *Mater. Lett.*, 2015, **138**, 175.

15 F. J. Himpsel, J. A. Knapp, J. A. VanVechten and D. E. Eastman, *Phys. Rev. B*, 1979, **20**, 624.

16 S. Drijkoningen, S. D. Janssens, P. Pobedinskas, S. Koizumi, M. K. Van Bael and K. Haenen, *Sci. Rep.*, 2016, **6**, 35667.

17 W. Janssen, S. Turner, G. Sakr, F. Jomard, J. Barjon, G. Degutis, Y. G. Lu, J. D'Haen, A. Hardy, M. K. Van Bael, J. Verbeeck, G. Van Tendeloo and K. Haenen, *phys. stat. sol.*, 2014, **8**, 705.

18 W. Yuan, L. Fang, Z. Feng, Z. Chen, J. Wen, Y. Xiong and B. Wang, *J. Mater. Chem. C*, 2016, **4**, 4778

View Article Online
DOI: 10.1039/C7NR06774G

19 T. Sugino, C. Kimura, K. Kuriyama, Y. Yokota, S. Koizumi and M. Kamo, *phys. stat. sol. (a)*, 1999, **174**, 145.

20 N. Roy, Y. Hirano, H. Kuriyama, P. Sudhagar, N. Suzuki, K. Katsumata, K. Nakata, T. Kondo, M. Yuasa, I. Serizawa, T. Takayama, A. Kudo, A. Fujishima and C. Terashima, *Sci. Rep.*, 2016, **6**, 38010.

21 S. Turner, Y. G. Lu, S. D. Janssens, F. D. Pieve, D. Lamoen, J. Verbeeck, K. Haenen and P. Wagner, G. V. Tendeloo, *Nanoscale,* 2012, **4**, 5960.

22 A. C. Ferrari, J. C. Meyer, V. Scardaci, C. Casiraghi, M. Lazzeri, F. Mauri, S. Piscanec, D. Jiang, K. S. Novoselov, S. Roth and A. K. Geim, *Phys. Rev. Lett.*, 2006, **97**, 187401.

23 G. Kalita, K. Wakita and M. Umeno, *RSC Adv.*, 2012, **2**, 2815.

24 S. Polyakov, V. Denisov, B. Mavrin, A. Kirichenko, M. Kuznetsov, S. Y. Martyushov, S. Terentiev and V. Blank, *Nanoscale Research Lett.*, 2016, **11**, 1.

25 Y. F. Chen, *Surf. Sci.*, 1997, **380**, 199.

26 P. T. Joseph, N. H. Tai, C. Y. Lee, H. Niu, W. F. Pong, and I. N. Lin, *J. Appl. Phys.,* 2008*,* **103**, 043720.

27 J. Ozaki, N. Kimura, T. Anahara and A. Oya, *Carbon*, 2007, **45**, 1847.

28 K. Yu, Z. Bo, G. Lu, S. Mao, S. Cui, Y. Zhu, X. Chen, R. S. Ruoff and J. Chen, *Nanoscale Research Lett.*, 2011, **6**, 202

29 R. H. Fowler and L. Nordheim, *Proc. R. Soc. London, Ser. A.*, 1928, **119**, 173.

30 Y. W. Zhu, H. Z. Zhang, X. C. Sun, S. Q. Feng, J. Xu, Q. Zhao, B. Xiang, R. M. Wang and D. P. Yu, *Appl. Phys. Lett.,* 2003, **83**, 144.

31 B. Xiang, Y. Zhang, Z. Wang, X. H. Luo, Y. W. Zhu, H. Z. Zhang and D. P. Yu, *J. Phys. D: Appl. Phys.,* 2005, **38**, 1152.

View Article Online
DOI: 10.1039/C7NR06774G

32 Z. S. Wu, S. Z. Deng, N. S. Xu, J. Chen, J. Zhou and J. Chen, *Appl. Phys. Lett.*, 2002, **80**, 3829.

33 J. Chen, S. Z. Deng, N. S. Xu, S. Wang, X. Wen, S. Yang, C. Yang, J. Wang and W. Ge, *Appl. Phys. Lett.,* 2002, **80**, 3620.

34 L. A. Valentín, J. Carpena-Nuñez, D. Yang and L. F. Fonseca, *J. Appl. Phys.*, 2013, **113**, 014308.

35 J. Liu, V. V. Zhirnov, A. F. Myers, G. J. Wojak, W. B. Choi, J. J. Hren, S. D. Wolter, M. T. McClure, B. R. Stoner and J. T. Glass, *J. Vac. Sci. Technol. B*, 1995, **13**, 422.

36 S. M. Song, J. K. Park, O. J. Sul and B. J. Cho, *Nano Lett.*, 2012, **12**, 3887.

37 K. J. Sankaran, T. H. Chang, S. K. Bikkarolla, S. S. Roy, P. Papakonstantinou, S. Drijkoningen, P. Pobedinskas, M. K. Van Bael, N. H. Tai, I. N. Lin and K. Haenen, *RSC Adv.*, 2016, **6**, 63178.

38 K. J. Sankaran, D. Q. Hoang, S. Korneychuk, S. Kunuku, J. P. Thomas, P. Pobedinskas, S. Drijkoningen, M. K. Van Bael, J. D'Haen, J. Verbeeck, K. C. Leou, K. T. Leung, I. N. Lin and K. Haenen, *RSC Adv.,* 2016, **6**, 90338

39 K. J. Sankaran, K. Srinivasu, K. C. Leou, N. H. Tai and I. N. Lin, *Appl. Phys. Lett.*, 2013, **103**, 251601.

40 K. J. Sankaran, S. Kunuku, B. Sundaravel, P. Y. Hsieh, H. C. Chen, K. C. Leou, N. H. Tai and I. N. Lin, *Nanoscale*, 2015, **7**, 4377.

41 K. J. Sankaran, M. Afsal, S. C. Lou, H. C. Chen, C. Chen, C. Y. Lee, L. J. Chen, N. H. Tai and I. N. Lin, *Small*, 2014, **10**, 179.

42 S. Kunuku, K. J. Sankaran, C. Y. Tsai, W. H. Chang, N. H. Tai, K. C. Leou and I. N. Lin, *ACS Appl. Mater. Interfaces*, 2013, **5**, 7439.

View Article Online
DOI: 10.1039/C7NR06774G

43 K. J. Sankaran, C. J. Yeh, S. Drijkoningen, P. Pobedinskas, M. K. Van Bael, K. C. Leou, I. N. Lin and K. Haenen, *Nanotechnology*, 2017, **28**, 065701.

44 L. Cui, J. Chen, B. Yang, D. Sun and T. Jiao, *Appl. Surf. Sci.*, 2015, **357**, 1.

45 T. C. Hung, C. F. Chen and W. T. Whang, *Diamond Relat. Mater.*, 2009, **18**, 443.

46 S. Shimada, K. Teii and M. Nakashima, *Diamond Relat. Mater.*, 2010, **19**, 956.

47 P. H. Talemi and G. P. Simon, *Carbon*, 2011, **49**, 2869.

48 D. Banerjee, S. Mukherjee and K. K. Chattopadhyay, *Appl. Surf. Sci.*, 2011, **257**, 3717.

49 D. Banerjee and K. K. Chattopadhyay, *Mater. Res. Bull.*, 2012, **47**, 3868.

50 J. Deng, R. Zheng, Y. Yang, Y. Zhao and G. Cheng, *Carbon*, 2012, **50**, 4732.

51 D. Banerjee, N. S. Das and K. K. Chattopadhyay, *Appl. Surf. Sci.*, 2012, **261**, 223.

52 C. X. Zhao, Y. Zhang, S. Z. Deng, N. S. Xu and J. Chen, *J. Alloys and Compounds*, 2016, **672**, 433.

53 I. L. Chang, P. H. Tsai and H. Y. Tsai, *Diamond Relat. Mater.*, 2016, **69**, 229.

54 Y. Wang, Q. Wei, Z. Yu, H. Long, Z. Deng, Y. Xie, J. Li, C. T. Lind, L. Mab and K. Zhou, *Appl. Surf. Sci.*, 2017, **423**, 788.

55 O. Chubenko, S. S. Baturin and S. V. Baryshev, *Appl. Phys. Lett.*, 2016, **109**, 113102.

56 R. L. Harniman, O. J. L. Fox, W. Janssen, S. Drijkoningen, K. Haenen and P. W. May, *Carbon*, 2015, **94**, 386.

57 P. Kovarik, E. B. D. Bourdon and R. H. Prince, *Phys. Rev B*, 1993, **48**, 12123.

58 S. Prawer, J. L. Peng, J. O. Orwa, J. C. McCallum, D. N. Jamieson and L. A. Bursill, *Phys. Rev. B.*, 2000, **62**, R16360.

59 S. S. Chen, H. C. Chen, W. C. Wang, C. Y. Lee and I. N. Lin, *J. Appl. Phys.*, 2013, **113**, 113704.

View Article Online
DOI: 10.1039/C7NR06774G

60 J. Kurian, K. J. Sankaran, J. P. Thomas, N. H. Tai, H. C. Chen and I. N. Lin, *J. Phys. D: Appl. Phys.,* 2014, **47**, 415303.

61 A. V. Generalov and Y. S. Dedkov, *Carbon*, 2012, **50**, 183.

62 K. Ostrikov, *J. Phys. D: Appl. Phys.*, 2011, **17**, 44.

63 N. Barekzi and M. Laroussi, *Plasma Processes Polym.*, 2013, **10**, 1039.

64 R. Satoa, D. Yasumatsua, S. Kumagai, K. Takeda, M. Hori and M. Sasaki, *Sens. Actuators A*, 2014, **215**, 144.

65 M. L. Terranova, S. Orlanducci, M. Rossi and E. Tamburri, *Nanoscale*, 2015, **7**, 5094.

66 J. Palomino, D. Varshney, O. Resto, B. R. Weiner and G. Morell, *ACS Appl. Mater. Interfaces*, 2014, **6**, 13815.

67 A. Pandey, A. Prasad, J. Moscatello and Y. K. Yap, *ACS Nano*, 2010, **4**, 6760.

68 M. W. Geis, N. N. Efremow, K. E. Krohn, J. C. Twichell, T. M. Lyszczarz, R. Kalish, J. A. Greer and M. D. Tabat, *Nature*, 1998, **393**, 431.

69 T. H. Chang, S. Kunuku, Y. J. Hong, K. C. Leou, T. R. Yew, N. H. Tai and I. N. Lin, *ACS Appl. Mater. Interfaces*, 2014, **6**, 11589.

70 H. Zanin, P. W. May, M. H. M. O. Hamanaka and E. J. Corat, *ACS Appl. Mater. Interfaces*, 2013, **5**, 12238.

71 K. A. Dean, T. P. Burgin and B. R. Chalamala, *Appl. Phys. Lett.*, 2001, **79**, 1873.

72 V. Venkatraman, A. Garg and D. Peroulis, *Appl. Phys. Lett.*, 2012, **100**, 083503.

73 A. Venkattraman, *Phys. Plasmas*, 2015, **22**, 057102.

74 K. Siuzdak, M. Ficek, M. Sobaszek, J. Ryl, M. Gnyba, P. Niedziałkowski, N. Malinowska, J. Karczewski and R. Bogdanowicz, *ACS Appl. Mater. Interfaces*, 2017, **9**, 12982.

View Article Online
DOI: 10.1039/C7NR06774G

75 K. J. Sankaran, K. Srinivasu, H. C. Chen, C. L. Dong, K. C. Leou, C. Y. Lee, N. H. Tai and I. N. Lin, *J. Appl. Phys.*, 2013, **114**, 054304.

76 M. Sobaszek, K. Siuzdak, J. Ryl, M. Sawczak, S. Gupta, S. B. Carrizosa, M. Ficek, B. Dec, K. Darowicki,and R. Bogdanowicz, *J. Phys. Chem. C.,* 2017, **121**, 20821.

77 J. Robertson, *Mater. Sci Engg. R.*, 2002, **37**, 129.

78 B. S. Truscott, M. W. Kelly, K. J. Potter, M. N. R. Ashfold and Y. A. Mankelevich, *J. Phys. Chem. A.,* 2016, **120**, 8537.

79 Z. Yiming, F. Larsson and K. Larsson, *Theor. Chem. Acc.*, 2014, **133**, 1432.

80 H. Li, J. Li, Z. Wang, and G. Zou, *Chem. Phys. Lett.* 2012, **550**, 130.

81 A. Wisitsoraat, W. P. Kang, J. L. Davidson, Q. Li, J. F. Xu and D. V. Kerns, *Appl. Surf. Sci.*, 1999, **146**, 280.

82 S. J. Kwon, Y. H. Shin, D. M. Asalm, and J. D. Lee, *J. Vac. Sci. Technol. B*, 1998, **16**, 712.

83 Y. C. Lee, S. J. Lin, I. N. Lin and H. F. Cheng, *J. Appl. Phys.*, 2005, **97**, 054310.

84 J. D. Carey, R. D. Forrest and S. R. P. Silva, *Appl. Phys. Lett.*, 2001, **78(16)**, 2339.

85 A. Ilie, A. C. Ferrari, T. Yagi, S. E. Rodil, J. Robertson, E. Barborini and P. Milani, *J. Appl. Phys.*, 2001, **90**, 2024.

86 A. Ilie, A. C. Ferrari, T. Yagi and J. Robertson, *Appl. Phys. Lett.*, 2000, **76**, 2627.

87 K. Panda, J. H. Jeong, J. Y. Park, K. J. Sankaran, B. Sundaravel and I. N. Lin, *Sci. Rep.*, 2017, **7**, 16325.

View Article Online
DOI: 10.1039/C7NR06774G

Table I. Key field electron emission performance parameters of MLG-BDD hybrid nanowall materials compared to (a) diamond-based hybrid nanostructures and (b) carbon nanoflakes/nanowalls structures reported in literature.

	Materials	E_0 (V/μm)	J_{FEE} (mA/cm^2)	β	lifetime
(a)	Diamond-graphene nanoflakes[37]	9.3	2.57 @ 24.0 V/μm	2380	---
	hBN-diamond nanorods[38]	6.0	4.10 @ 14.0 V/μm	5870	435 min
	Diamond-CNTs[39]	2.1	0.006 @ 2.7 V/μm	2566	250 min
	Gold-UNCD hybrids[40]	2.1	5.30 @ 4.9 V/μm	---	372 min
	UNCD-ZnO nanorods[41]	2.08	5.5 @ 4.25 V/μm	4227	140 min
	MCD nanocones[42]	35.0	0.91 @ 200 V/μm	259	---
	NCD nanotips[42]	16.2	2.50 @ 38 V/μm	347	---
	UNCD nanopillars[42]	11.6	3.95 @ 30 V/μm	3041	---
	Few-layer graphene-diamond nanorods[43]	4.21	2.24 @ 10 V/μm	3480	---
	Diamond nanorods[43]	7.26	0.60 @ 15.1 V/μm	2326	---
(b)	Carbon nanowalls[44]	4.7	3.4 @ 7.0 V/μm	1399	240 min
	Petal-like carbon nanotubes[45]	2.7	---	---	---
	Nitrogen incorporated carbon nanowalls[46]	3.0	---	2000	---
	Graphene nanowalls[47]	1.2	---	14.2 x 1000	---
	Amorphous carbon nanowalls[48]	1.4	---	8500	---
	Carbon nanofern-like structure[49]	4.8	---	748	---
	Graphene-carbon nanotube hybrids[50]	0.98	---	3980	20 h
	Carbon nanoflakes coated Si nanowires[51]	2.77	---	---	---
	Few-layer graphene nanowalls[52]	4.6	---	1450	6000 s
	Carbon nanotubes-carbon nanoflake balls[53]	1.77	---	7932	50 h
	Caterpillar-like structural carbon film[54]	3.66	---	1970	100 min
(c)	MLG-BDD hybrid nanowalls[Present study]	2.4	4.2 @ 4.0 V/μm	4500	700 min

View Article Online
DOI: 10.1039/C7NR06774G

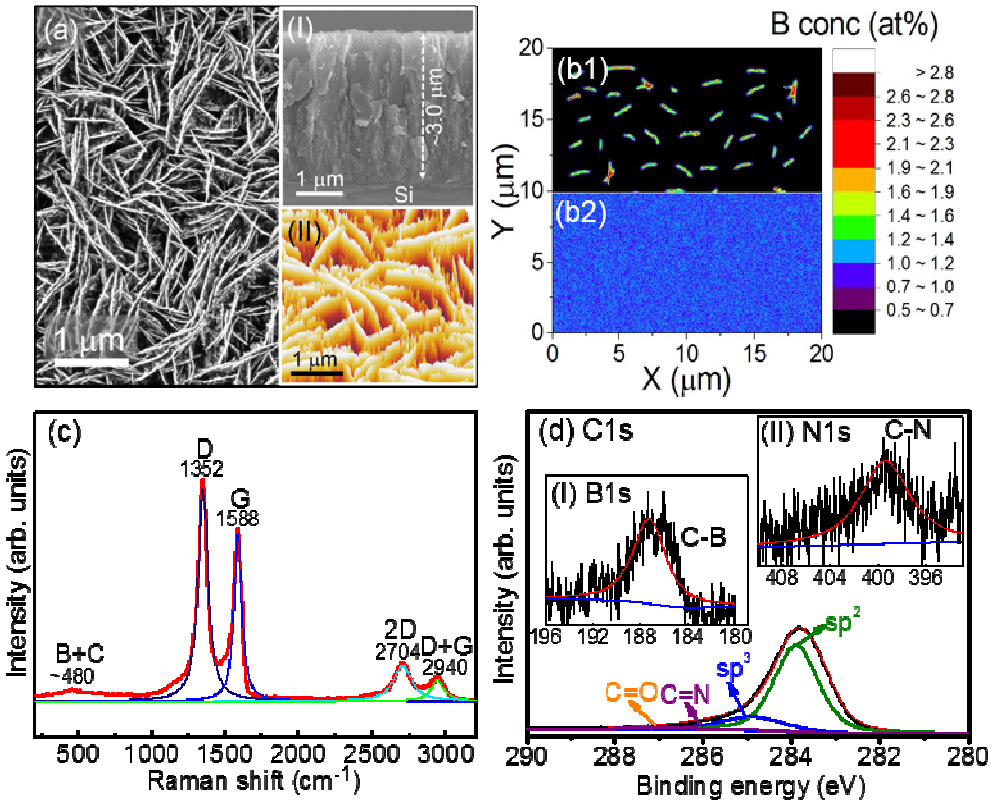

Fig. 1 a) SEM image of MLG-BDD hybrid nanowall materials and the corresponding cross-sectional SEM image (inset "I") and 3D reconstruction of surface morphology (inset "II"). b) SIMS mapping taken from the top (b1) and bottom (b2) parts of the nanowalls. c) Deconvoluted visible-Raman (λ = 514 nm) spectrum of MLG-BDD hybrid nanowall materials. d) C1s XPS spectrum of MLG-BDD hybrid nanowall materials along with B1s (inset "I") and N1s (inset "II") XPS spectra of the materials.

View Article Online
DOI: 10.1039/C7NR06774G

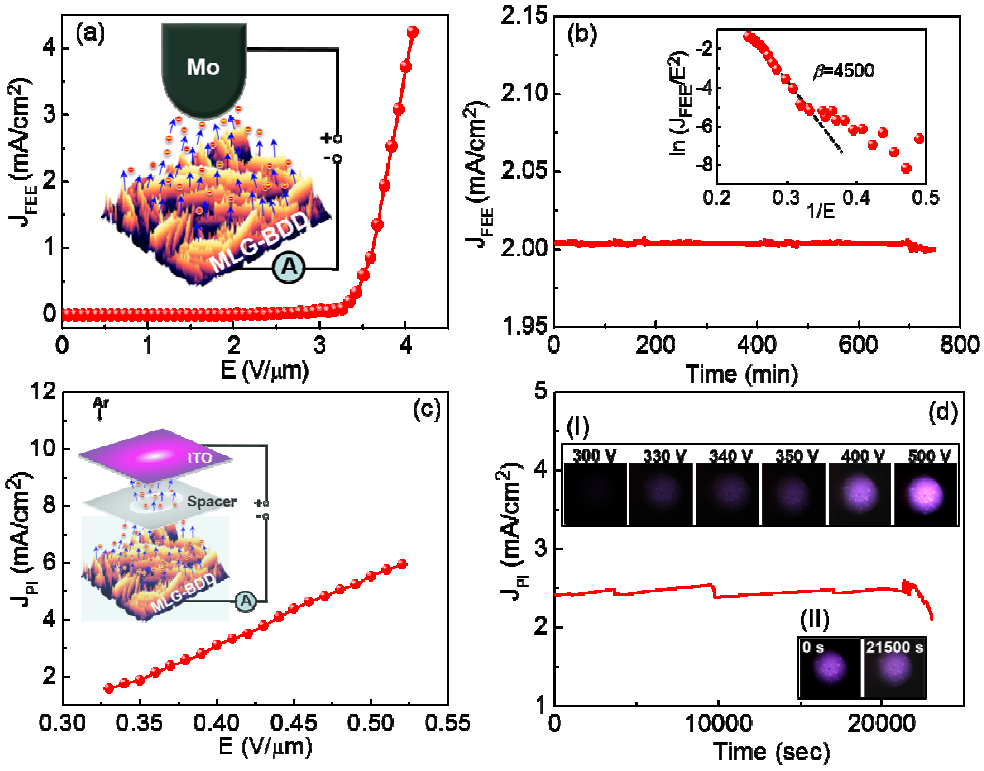

Fig. 2 a) Field electron emission (FEE) current density (J_{FEE}) as a function of applied field (E) for MLG-BDD hybrid nanowall materials with the inset showing the schematic of the FEE measurement. b) The lifetime stability test, J_{FEE} versus time curve, for the materials with inset showing the F-N plot corresponding J_{FEE}–E characteristic curve shown in "a". c) The plasma current density versus applied field of a microplasma cavity, which utilized ITO coated glass as anode and MLG-BDD hybrid nanowall materials as cathode materials. The inset of (c) shows the schematic of plasma illumination measurement set-up. d) The plasma illumination stability of the nanowalls. Inset I shows the photographs of plasma illumination characteristics of the microplasma devices at varying voltages and inset "II" shows the plasma illumination intensity at 0 s and 21500 s after ignition of plasma, revealing that the plasma device is essentially not degraded even after long time services.

View Article Online
DOI: 10.1039/C7NR06774G

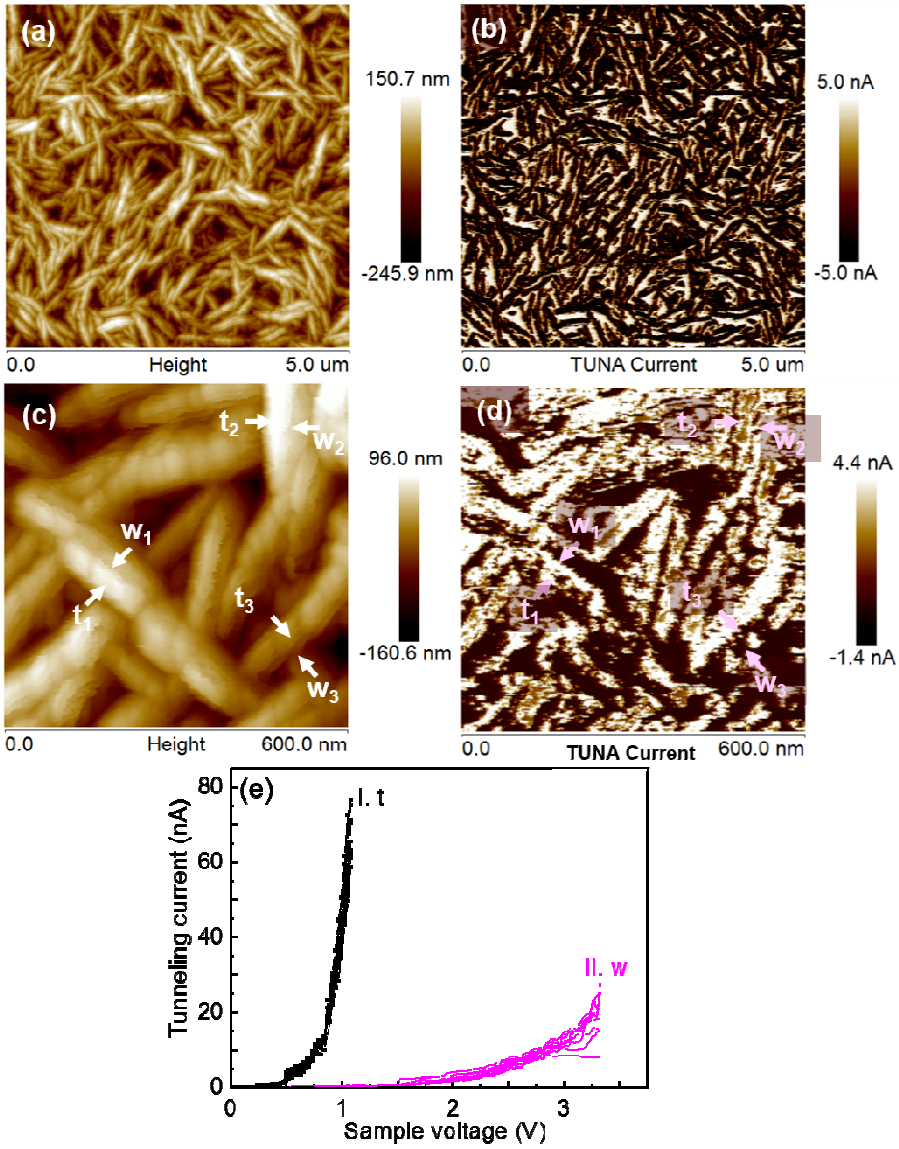

Fig. 3 a) AFM image of MLG-BDD hybrid nanowall materials and b) the corresponding PF-TUNA image acquired at -1 V. c) High resolution AFM and d) the corresponding PF-TUNA images of the MLG-BDD hybrid nanowall materials acquired at -2 V. e) Local electron tunneling curves, the I−V curves, at (I) the top edges and (II) the side walls of MLG-BDD hybrid nanowall materials.

View Article Online
DOI: 10.1039/C7NR06774G

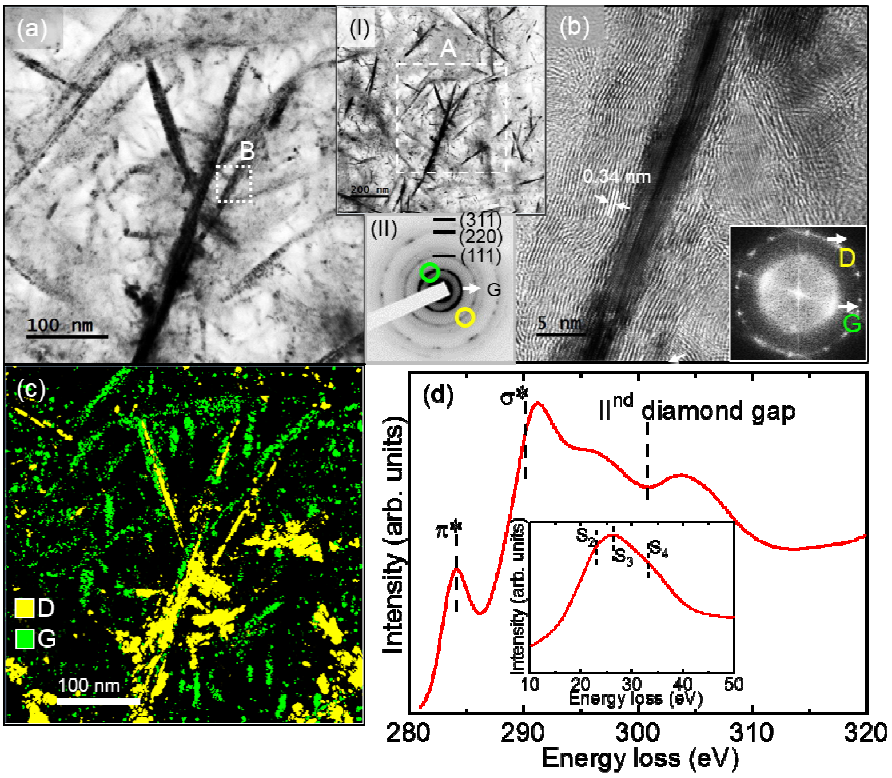

Fig. 4 a) A high magnification bright field TEM (BF-TEM) micrograph of the MLG-BDD hybrid nanowall materials corresponding to region "A" designated in the low magnification BF-TEM image, which is shown as inset "I" in "a", whereas the corresponding SAED pattern is shown as inset "II". b) High resolution TEM micrograph, the structure image, taken at the region marked as "B" in "a" with the Fourier transformed diffractogram corresponding to entire structure image shown as inset. c) The composed dark field image corresponding TEM micrograph in "a" to mark the diamond and graphene regimes. d) Core-loss EELS spectrum of the MLG-BDD hybrid nanowall materials corresponding to BF-TEM micrograph in "a", along with plasmon loss EELS spectrum of the materials shown as inset.

View Article Online
DOI: 10.1039/C7NR06774G

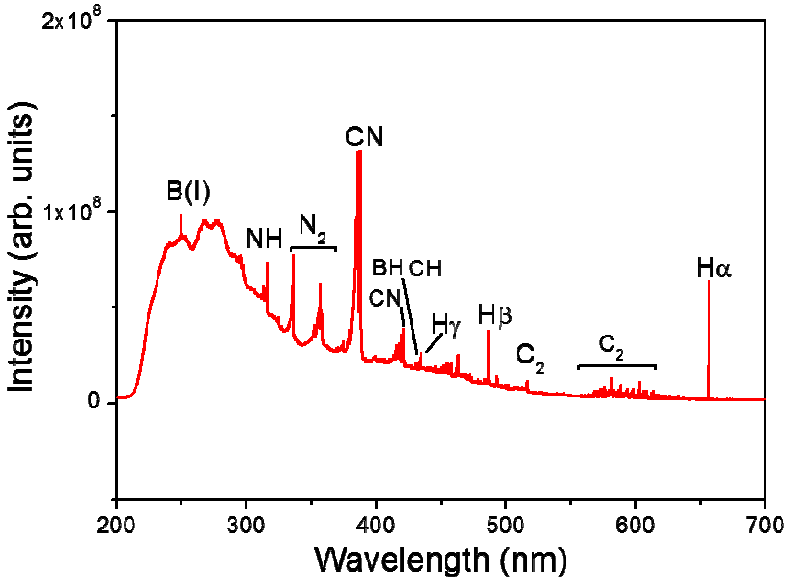

Fig. 5 Optical emission spectrum of the $H_2/CH_4/B_2H_6/N_2$ plasma used for growing MLG-BDD hybrid nanowall materials by the MWPECVD process.

View Article Online
DOI: 10.1039/C7NR06774G

Graphical abstract

Enhancement in field electron emission (FEE) behavior of a hybrid structure of self-organized multilayered graphene (MLG)–boron doped diamond (BDD) nanowall materials, is observed. FEE properties of MLG-BDD hybrid nanowalls show a low turn-on field of 2.4 V μm^{-1} with high current density of 4.2 mA cm^{-2} (at an applied field of 4.0 V μm^{-1}), a large field enhancement factor of 4500 and a good current stability of 700 min, which are better than those of other carbon-based hybrid FEE materials The potential application of this high performance FEE material is demonstrated by the plasma illumination measurements for a microplasma device and opens new prospects in flat panel displays and high brightness electron sources.